International Journal of Bifurcation and Chaos, Vol. 14, No. 8 (2004) 2867–2873

CHAOS IN A NONLINEAR ANALOG COMPUTER

KEN KIERS*, TIM KLEIN†, JEFF KOLB‡ and STEVE PRICE§
Physics Department, Taylor University,
236 West Reade Ave., Upland, IN 46989, USA
**knkiers@tayloru.edu*
†*klein@physics.umn.edu*
‡*jkolb@darkwing.uoregon.edu*
§*price@physics.montana.edu*

J. C. SPROTT
Department of Physics, University of Wisconsin,
1150 University Ave., Madison, WI 53706, USA
sprott@physics.wisc.edu

Received June 27, 2003; Revised August 1, 2003

We explore the chaotic behavior of a nonlinear electrical circuit constructed with simple components such as diodes and linear operational amplifiers. The circuit may be regarded as a nonlinear analog computer that gives a nearly exact solution of a particular chaotic model. Detailed comparisons between theoretical and experimental bifurcation points and power spectra yield differences of less than 1%.

Keywords: Electronic chaos; nonlinear analog computer.

The recent study of nonlinear dynamical systems has led to many intriguing and surprising results. One of these is the observation that certain systems can exhibit chaos, where small initial uncertainties grow exponentially in time giving large uncertainties in the future state of the system. Many examples of chaos have been found in nature and in numerical solutions of iterated maps and differential equations. However, the equations often poorly represent the phenomena they model and the agreement is usually at best qualitative. This paper reports a comparison between a simple model and an actual experiment with agreement that is better than 1% for such quantities as bifurcation points and power spectra.

We consider a time-continuous system described by an autonomous ordinary differential equation (ODE) in a single variable, where the minimal conditions for chaos are that the ODE be third-order and contain a nonlinearity. Several authors have searched for the simplest third-order ODE that exhibits chaos [Gottlieb, 1996; Linz, 1997; Sprott, 1997; Linz & Sprott, 1999; Sprott, 2000a, 2000b]. One of the simplest of such systems uses the absolute value nonlinearity and is given by [Linz & Sprott, 1999]

$$\dddot{x} = -A\ddot{x} - \dot{x} + |x| - 1\,, \tag{1}$$

where A is the control parameter. Equation (1) has a stable fixed point when $A > 1$ and undergoes a Hopf bifurcation at $A = 1$. The solutions follow a

†Current address: School of Physics and Astronomy, University of Minnesota, Minneapolis, MN 55455, USA.
‡Current address: Department of Physics, University of Oregon, Eugene, OR 97403-5203, USA.
§Current address: Department of Physics, Montana State University, Room 264 EPS Building, Bozeman, MT 59717, USA.

period-doubling route to chaos as A is lowered from 1 to 0.64085 [Linz & Sprott, 1999]. For A in the range 0.64085 to about 0.547 the solutions exhibit a very detailed structure with chaotic bands interrupted by periodic windows [Linz & Sprott, 1999].

As noted by Sprott [2000a, 2000b], Eq. (1) belongs to a class of third-order ODEs that may be represented by simple electronic circuits with the variable x corresponding to the voltage at a node in the circuit. Although such a circuit provides an analog simulation of a differential equation, it should be noted that the power and energy flow among individual elements in such a circuit are not physically meaningful. (This may be contrasted with a physical circuit, in which the power flow has a well-defined physical meaning, as in a physical spring-mass system.) The circuits in [Sprott, 2000a] and [Sprott, 2000b] contain operational amplifiers and (in some cases) diodes, which produce nonlinearities and permit chaos. Resistors or other elements may be used as control parameters to bring the circuits into or out of chaos, and the circuits may be scaled over many orders of magnitude in frequency, making them ideal for demonstration and study. Our choice of component values puts the typical frequencies in the range of a few Hertz, allowing for accurate data measurement and storage. Note that the circuits in [Sprott, 2000a, 2000b] are similar to Chua's circuit [Matsumoto *et al.*, 1985, 1987], although Chua's circuit has a very complicated representation in terms of $\dddot{x}$, and it is not straightforward to scale to different frequencies because it (typically) contains an inductor.[1]

Figure 1 shows the circuit considered here. Its modular design permits insertion of different nonlinear subcircuits in the box denoted "$D(x)$." The circuit contains three successive inverting integrators with global feedback and may be viewed as a nonlinear analog computer. Simple elements within the box (such as diodes and operational amplifiers) provide the nonlinearity required for chaos. The elements are arranged such that the voltage at the output of the box (on the left) is related to its input by $V_{\rm out} = D(V_{\rm in})$. A similar modular design was described in [Sprott, 2000b], where chaos was observed for several different functions $D(x)$. Assuming nominal values for the resistors ($R = 47$ kΩ) and capacitors ($C = 1$ μF) yields the following differential equation for the voltage at the node "x" in the figure,

$$\dddot{x} = -\left(\frac{R}{R_v}\right)\ddot{x} - \dot{x} + D(x) - \left(\frac{R}{R_0}\right)V_0\,, \quad (2)$$

where the input voltage V_0 could have either polarity. In Eq. (2) $\dot{x}$ represents differentiation with respect to the dimensionless quantity $\tilde{t} = t/(RC)$, and R_v is the variable resistor in Fig. 1. This resistor is the control parameter that brings the system into or out of chaos and allows for a detailed quantitative study.

We construct and analyze one example from the class of circuits noted above using the subcircuit in Fig. 2 described in [Horowitz & Hill, 1989]. To a very good approximation, the relation between the input and output of the subcircuit is given by

$$\begin{aligned} V_{\rm out} &= D(V_{\rm in}) \\ &= \begin{cases} \left[\dfrac{R_3R_5}{R_2R_4} - \dfrac{R_5}{R_1}\right]V_{\rm in}, & V_{\rm in} > 0\,, \\ -\left[\dfrac{R_5}{R_1}\right]V_{\rm in}, & V_{\rm in} < 0\,. \end{cases} \end{aligned} \quad (3)$$

For $R_1 = R_2 = R_3 = R_5 = 2R_4$, the subcircuit yields an absolute value nonlinearity, $D(x) = |x|$. With this $D(x)$ and with $V_0 = 0.25$ V and $R_0 = R$, Eq. (2) is equivalent to Eq. (1), except for a trivial change in the constant term.[2] A simpler

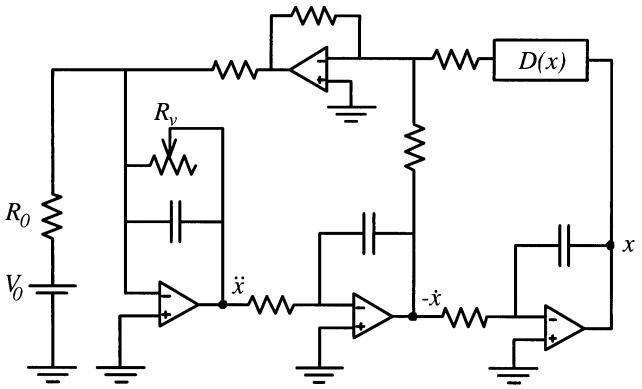

Fig. 1. Schematic diagram of the circuit described by Eq. (2). The box labeled "$D(x)$" represents a subcircuit comprised of simple elements such as diodes and linear operational amplifiers. Nominal values for the unlabeled resistors and capacitors are $R = 47$ kΩ and $C = 1$ μF.

[1] Variants of Chua's circuit that do not use inductors may be found, e.g. in [Tôrres & Aguirre, 2000; Elwakil & Kennedy, 2000; Elwakil & Kennedy, 2001].

[2] In the numerical calculations we use measured resistor, capacitor and voltage values, resulting in small changes in the terms in Eq. (2).

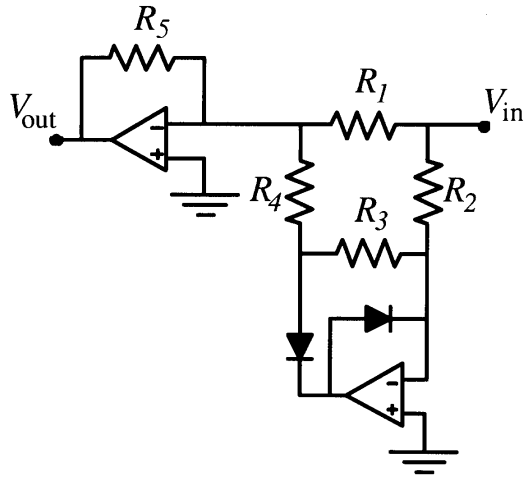

Fig. 2. Schematic diagram of the subcircuit shown in Fig. 1 that gives $V_{\rm out} = D(V_{\rm in}) = |V_{\rm in}|$ if $R_1 = R_2 = R_3 = R_5 = 2R_4$. Silicon diodes are used in the experiment.

Table 1. Comparison between several experimental and theoretical values of $V_{\rm out}$ for the subcircuit shown in Fig. 2. The theoretical values are obtained from Eq. (3), using measured values for the various resistances. All entries in the Table are in units of mV.

$V_{\rm in}$	$V_{\rm out}$ (Exp.)	$V_{\rm out}$ (Theory)	Difference
−690	690	689	1
−100.0	100.9	99.8	1.1
−31.9	33.0	31.8	1.2
−12.7	13.8	12.7	1.1
−4.1	5.3	4.1	1.2
2.1	4.9	2.1	2.8
12.8	15.6	12.8	2.8
32.1	34.9	32.1	2.8
100.0	102.9	100.1	2.8
690	694	690	4

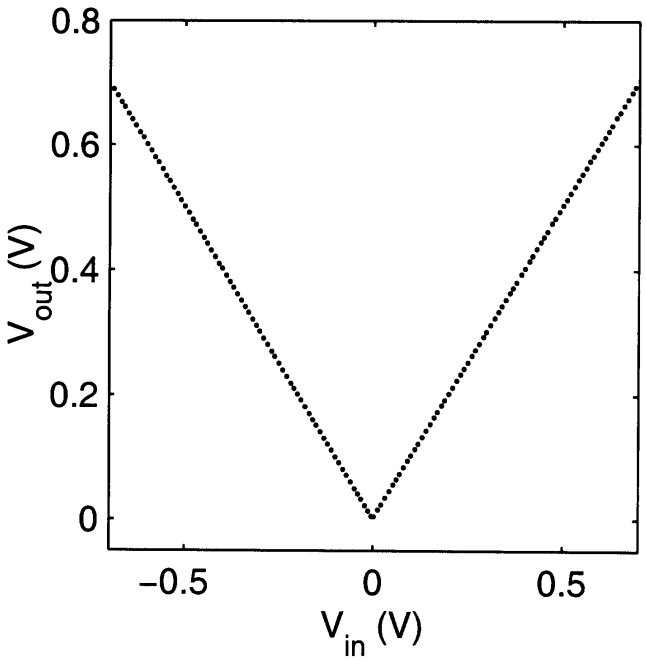

Fig. 3. Experimental plot of $V_{\rm out}$ versus $V_{\rm in}$ for the subcircuit shown in Fig. 2.

electronic representation of Eq. (1) — using two diodes, but fewer linear components — was described in [Sprott, 2000a]. The advantage of the present circuit is that it provides an almost ideal absolute value nonlinearity, whereas the nonlinearity in the former circuit contained a "dead" region bounded by two "knees" (due to the I–V characteristic of the diodes). The "knees" in the simpler arrangement are difficult to model theoretically due to their sensitive dependence on ambient laboratory conditions such as temperature. Figure 3 shows an experimental plot of $V_{\rm out}$ versus $V_{\rm in}$ for the subcircuit in Fig. 2. It is clear from the plot that the subcircuit provides an excellent approximation to the absolute value function, even at quite small values for the input voltage. Table 1 compares several experimental values of $V_{\rm out}$ to theoretical values obtained using Eq. (3). The experimental values tend to exceed the theoretical ones by approximately 1 mV for $V_{\rm in} < 0$ and 3 mV for $V_{\rm in} > 0$. The experimental values are observed to have a mild sensitivity (on the order of a few mV) to the supply voltage for the operational amplifiers and to the ambient conditions in the laboratory.

The variable resistor in Fig. 1 actually consists of a number of fixed resistors in combination with eight digital potentiometers. The digital potentiometers are in series with each other and in parallel with a fixed resistance. That combination is arranged in series with another fixed resistance. Each potentiometer has 256-step resolution over approximately 10 kΩ. The resulting combination of resistors and potentiometers yields approximately 2000-step resolution over the range of interest from approximately 57 kΩ to 84 kΩ, with increased resolution at the high end. Voltages at the nodes labeled "x" and "$-\dot{x}$" in Fig. 1 are sampled at a frequency of 166.7 Hz, which is sufficient to probe the interesting frequency range from 0 to approximately 20 Hz (c.f. Fig. 6). The Analog-to-Digital (A/D) conversion system is capable of 12-bit (4096-step) resolution over 0–5 V. The potentiometers are also

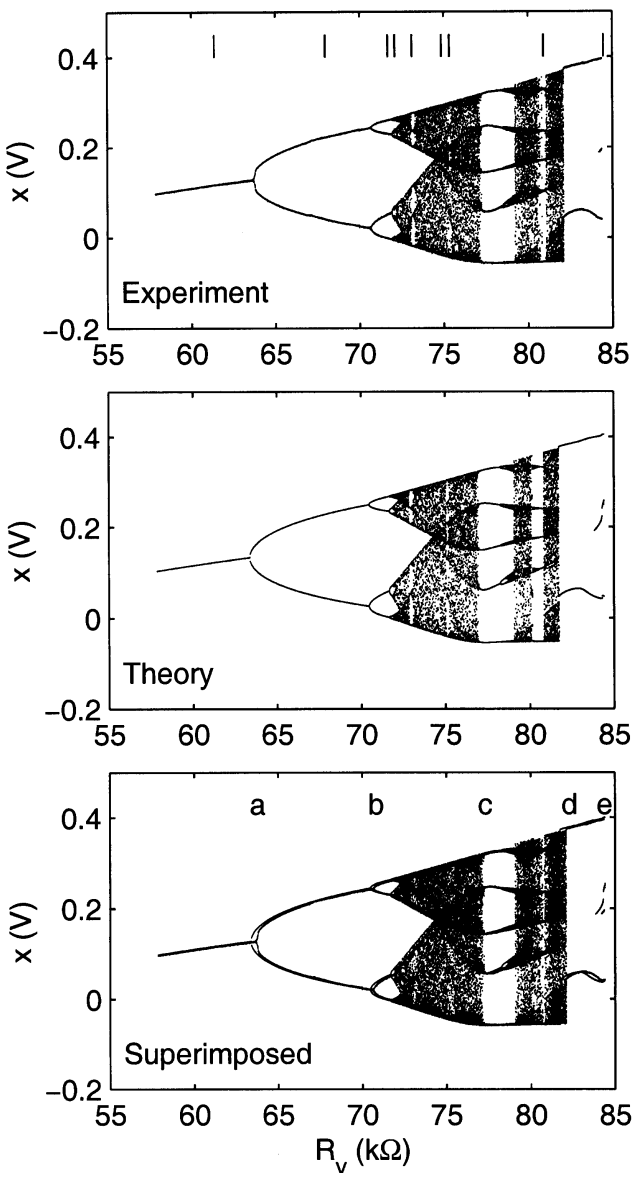

Fig. 4. Experimental, theoretical and superimposed bifurcation plots for the circuit in Figs. 1 and 2. In the superimposed plot, the theoretical plot has been shifted vertically by −5 mV. The short vertical lines in the top plot indicate the values of R_v for the phase space plots in Fig. 5. The labels a–e in the bottom plot denote the bifurcation points in Table 2.

designed to function between 0 and 5 V. The ground plane of the circuit is "floated" at approximately 3 V to help satisfy the various voltage range requirements. Furthermore, simple amplifiers are employed at the x and $-\dot{x}$ nodes to make optimal use of the 0 to 5 V range of the A/D converters.

Figure 4 shows experimental and theoretical bifurcation plots of local maxima as a function of R_v. For resistances much above 84 kΩ the solutions of Eq. (2) (with $D(x) = |x|$) become unbounded — and the operational amplifiers saturate — and for values much below 57 kΩ, the voltage approaches a stable fixed point. To generate the experimental plot (the top plot in Fig. 4) we identify candidate local maxima within the data set using a rough cut that compares triplets of x values. Further refinement includes a cubic polynomial fit to 21 points surrounding each candidate maximum in x. This method is very successful at identifying local maxima, distinguishing true maxima from "almost" saddle points and removing noise. In particular, the method works well near $R_v = 84$ kΩ, where the signal bifurcates from period-2 to period-3 as a saddle point turns into a new local maximum. A study of fits obtained in various cases indicates that true maxima are sometimes underestimated by up to about 5 mV, depending on the local shape of the curve. The theoretical plot (the middle plot in Fig. 4) is generated using a fourth-order Runge–Kutta with a step size of 0.25 ms. The resistance and capacitance measurements used in the theory are accurate to ±0.02%, with capacitance measurements performed at 12 Hz. Some of the details of the theoretical plot are extremely sensitive to the exact values used for the resistors and capacitors. For example, varying resistance and capacitance values within the allowed ±0.02% ranges causes the "middle" chaotic band near 80 kΩ to change in width or disappear. We have chosen values for the resistors and capacitors (within the allowed ranges) that produce a band much like the experimental one. The bottom superimposed plot in Fig. 4 shows remarkable agreement of theory and experiment.

Table 2 compares the experimental and theoretical bifurcation points labeled a–e in Fig. 4. The values for the bifurcation points differ by less than one percent, as indicated in the last column of the table, with the theoretical values slightly smaller than the experimental ones. This

Table 2. Comparison of theoretical and experimental bifurcation points. The labels a–e are indicated in the bottom plot in Fig. 4. Contributions to the quoted uncertainties are described in the text.

	Exp. (kΩ)	Theory (kΩ)	Diff. (kΩ)	Diff. (%)
a	63.62 ± 0.07	63.34 ± 0.08	0.28	0.44
b	70.65 ± 0.06	70.44 ± 0.11	0.21	0.30
c	77.18 ± 0.05	76.95 ± 0.20	0.23	0.30
d	82.11 ± 0.02	81.70 ± 0.15	0.41	0.50
e	84.20 ± 0.02	83.76 ± 0.13	0.44	0.52

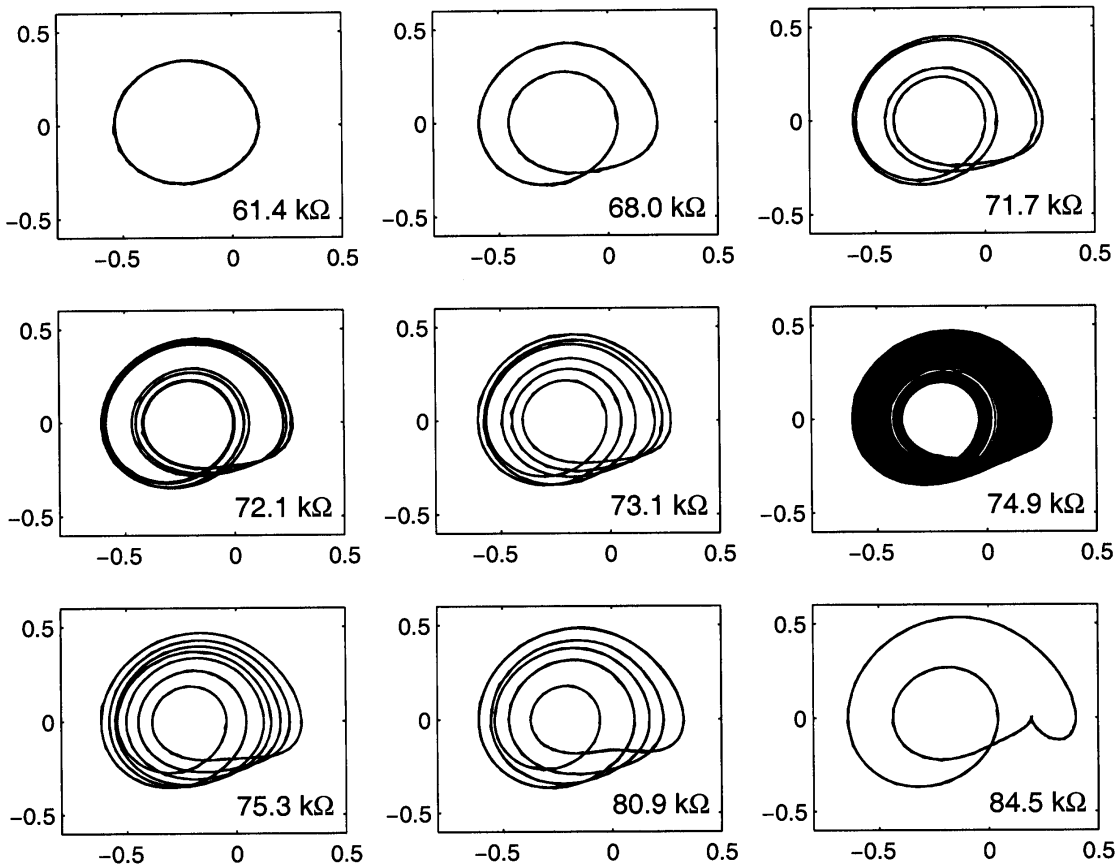

Fig. 5. Experimental phase space plots for various values of R_v. In each case $\dot{x}$ and x are plotted (in V) on the vertical and horizontal axes, respectively. The values of R_v are indicated in the lower-right corner of each plot and correspond to the short vertical lines in the top plot of Fig. 4. From left to right and top to bottom, the plots are period-1, -2, -4, -8, -6, chaos, period-7, -5 and -3.

trend is also evident in Fig. 4. There are several sources of uncertainty in determining the experimental bifurcation points included in the table. The experimental uncertainties include determining the bifurcation points from the plot, values of the fixed resistors in R_v ($\pm 0.02\%$ for each) and the digital potentiometers. The potentiometers are mildly nonlinear, but are calibrated at 3 V (the value of the floating ground) to mitigate the effect of nonlinearity. Nevertheless, this nonlinearity gives a small uncertainty, as does the calibration curve itself. The uncertainties in the theoretical bifurcation points are determined by choosing resistor and capacitor values in the theoretical model from a random Gaussian distribution with width 0.02%. In most cases, the errors between the experimental and theoretical bifurcation points in Table 2 exceed the expected errors, indicating that other experimental or theoretical uncertainties exist. Possible additional errors include the drifting of resistor or capacitor values (beyond their stated uncertainties) due to aging or environmental changes, small leakage currents in the operational amplifiers and slight departures from the idealized behavior assumed for the subcircuit in Fig. 2. Other studies of the circuit point to the first of these as the most likely remaining uncertainty.

A sampling of experimental phase space plots in Fig. 5 demonstrates the low noise in the circuit as well as some of the interesting periodic behavior that occurs in the narrow nonchaotic windows in Fig. 4. The first four plots (periods one, two, four and eight) demonstrate the period-doubling route to chaos evident in Fig. 4. The period-six, -seven and -five windows are discernible in both the experimental and theoretical bifurcation plots in Fig. 4, although the period-seven window is quite narrow. One of the three loops on the period-three attractor just barely crosses the $\dot{x} = 0$ line and looks almost like a cusp. For slightly smaller values of R_v the loop descends below the $\dot{x} = 0$ line and becomes a "bump," leaving a period-two phase space plot.

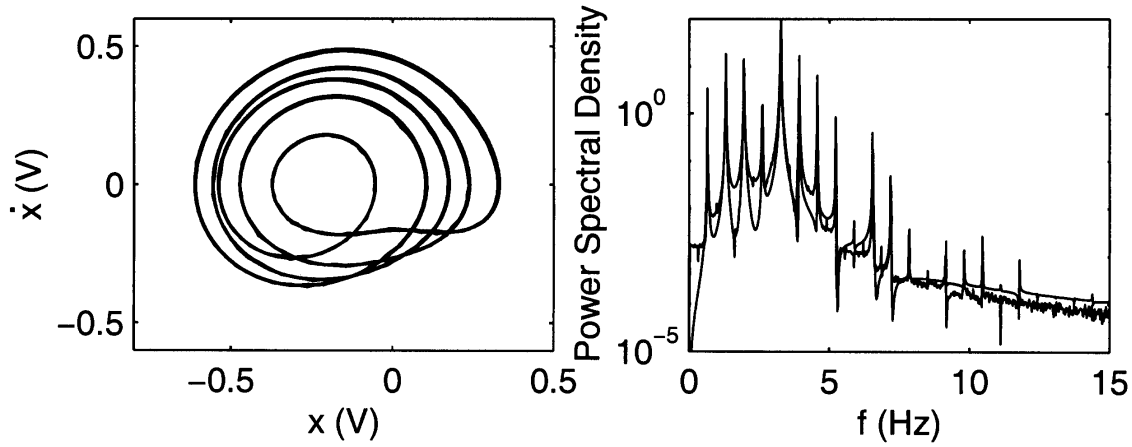

Fig. 6. Phase space and power spectral density for the period-five window near $R_v = 81$ kΩ. In each plot the theoretical and experimental results are superimposed. The theoretical result is discernible as the smoother of the two lines in the plot on the right.

The chaotic attractor in Fig. 5 is from the band near $R_v = 75$ kΩ.

Figure 6 shows a detailed comparison between theory and experiment for the period-five window near $R_v = 81$ kΩ. The theoretical results were generated using a slightly lower value for R_v (by approximately 0.27 kΩ), consistent with the shift evident in Fig. 4. On the scale shown, there is no discernible difference between the theoretical and experimental attractors, although small differences, of order 4–8 mV, exist. This agreement between theory and experiment is typical of that found for the attractors in Fig. 5. The theoretical and experimental frequency spectra in Fig. 6 also agree very well, as is typical of the cases examined. In this case, the experimental curve is the one containing a small amount of noise. The frequency spectrum has a dominant peak at 3.27 Hz and subdominant peaks at $n \times 3.27/5$ Hz, where $n = 1, 2, 3, 4, 6, 7, \ldots$. At low frequencies, the positions of the peaks agree to at least 0.01–0.02 Hz (which is the frequency resolution of the 8192-point FFT). At frequencies of order 10 Hz, the theoretical and experimental peaks differ by up to about 0.04 Hz, or about 0.4%.

The circuit described here has a modular design and may be considered as a nonlinear analog computer that uses simple components (ordinary diodes and linear operational amplifiers) to give an exact solution to a chaotic model. The ideal behavior of the nonlinearity in the circuit and the simplicity of the circuit itself allow for a very detailed comparison between theory and experiment. The circuit represents a new instrument for the detailed quantitative study of chaotic systems. One could couple two or more such circuits together and study a wide variety of complex phenomena such as synchronization, chaos control, routes to chaos or high-dimensional dynamics. Such studies have been performed in the past using other chaotic systems, but not to the accuracy permitted by this system [Madan, 1993]. The circuit is also ideal for lecture demonstration and student projects.

Acknowledgments

We would like to thank J. Goldberg, W. Holmes, H. Voss, J. Schea and K. Knapp for invaluable technical assistance and D. Schmidt for checking some of the results. K. Kiers was supported by an award from Research Corporation. J. Kolb and S. Price were supported by the Science Research Training Program at Taylor University.

References

Elwakil, A. S. & Kennedy, M. P. [2000] "Generic RC realizations of Chua's circuit," *Int. J. Bifurcation and Chaos* **10**, 1981–1985.

Elwakil, A. S. & Kennedy, M. P. [2001] "Construction of classes of circuit-independent chaotic oscillators using passive-only nonlinear devices," *IEEE Trans. Circuits Syst.-I* **48**, 289–307.

Gottlieb, H. P. W. [1996] "Question #38. What is the simplest jerk function that gives chaos?" *Am. J. Phys.* **64**, p. 525.

Horowitz, P. & Hill, W. [1989] *The Art of Electronics*, 2nd edition (Cambridge University Press, NY).

Linz, S. J. [1997] "Nonlinear dynamical models and jerky motion," *Am. J. Phys.* **65**, 523–526.

Linz, S. J. & Sprott, J. C. [1999] "Elementary chaotic flow," *Phys. Lett.* **A259**, 240–245.

Madan, R. N. [1993] *Chua's Circuit*: *A Paradigm for Chaos* (World Scientific, Singapore).

Matsumoto, T., Chua, L. O. & Komuro, M. [1985] "The double scroll," *IEEE Trans. Circuits Syst. CAS* **32**, 797–818.

Matsumoto, T., Chua, L. O. & Komuro, M. [1987] "Birth and death of the double scroll," *Physica* **D24**, 97–124.

Sprott, J. C. [1997] "Some simple chaotic jerk functions," *Am. J. Phys.* **65**, 537–543.

Sprott, J. C. [2000a] "Simple chaotic systems and circuits," *Am. J. Phys.* **68**, 758–763.

Sprott, J. C. [2000b] "A new class of chaotic circuit," *Phys. Lett.* **A266**, 19–23.

Tôrres, L. A. B. & Aguirre, L. A. [2000] "Inductorless Chua's circuit," *Electron. Lett.* **36**, 1915–1916.